PNAS RESEARCH ARTICLE | EARTH, ATMOSPHERIC, AND PLANETARY SCIENCES

Hillslope roughness reveals forest sensitivity to extreme winds

Tyler H. Doane[a,1], Brian J. Yanites[a], Douglas A. Edmonds[a], and Kimberly A. Novick[b]

Edited by Susan Brantley, Pennsylvania State University, University Park, PA; received July 14, 2022; accepted December 1, 2022

Windthrow, or the uprooting of trees by extreme wind gusts, is a natural forest disturbance that creates microhabitats, turns over soil, alters hydrology, and removes carbon from the above-ground carbon stock. Long recurrence intervals between extreme wind events, however, make direct observations of windthrow rare, challenging our understanding of this important disturbance process. To overcome this difficulty, we present an approach that uses the geomorphic record of hillslope topographic roughness as a proxy for the occurrence of windthrow. The approach produces a probability function of the number of annual windthrow events for a maximum wind speed, allowing us to explore how windthrow or tree strengths may change due to shifting wind climates. Slight changes to extreme wind speeds may drive comparatively large changes in windthrow production rates or force trees to respond and change the distribution. We also highlight that topographic roughness has the potential to serve as an important archive of extreme wind speeds.

topography | roughness | wind | trees

Significance

Extreme wind can cause trees to uproot leaving behind a pit and a mound. These windthrow disturbances affect forest ecology, geomorphology, and carbon fluxes. Windthrow frequency remains challenging to constrain because the extreme wind events that cause them are rare. Here, we suggest that forest floors can encode the topographic signature of wind because their surface roughness reflects the balance between windthrow production and topographic decay. We develop a probabilistic model that describes topographic roughness created by extreme wind events and use it to quantify the frequency of windthrow in southern Indiana. Our results suggest that the roughness of forest floors may be an archive of extreme wind speeds.

Wind imposes a common yet variable force on forests that can occasionally uproot trees. Turbulent sweeps deliver unusually high wind speeds over short durations into the canopy (1) and have the potential to impart drag forces that exceed the resistance strengths of roots and soil (2–5). When this happens, trees topple in a process known as tree or windthrow, which has consequences for geomorphology and forest ecosystems by transporting and mixing soil (6–11), creating canopy gaps (12, 13), and providing niche habitats (14, 15). Windthrow has an important role in ecosystem functioning of forests and has consequences at scales that range from local to global. Indeed, widespread windthrow is a potential explanation for the observed interannual variability in terrestrial carbon sinks (16, 17). Further, climate change may alter the frequency and magnitude of strong wind events (18), and windthrow frequencies will respond (19, 20).

Understanding the carbon cycle consequences of windthrow rates is particularly pressing given the emerging focus on nature-based climate change mitigation strategies like reforestation and altered forest management (21). Effectively implementing and evaluating nature-based climate solutions (NbCS) requires quantifying present-day carbon stocks and fluxes between them (22). Furthermore, we must know how climate feedback, like changing wind speeds, will change rates of tree mortality and threaten the residence time of carbon stored in forest biomass. Efforts to quantify rates of windthrow to evaluate its impact on carbon dynamics have historically faced challenges posed by the long recurrence interval and stochasticity of extreme events that drive it (23, 24). Here, we demonstrate that the topographic roughness of forests serves as an archive of windthrow events and can be used to quantify the process.

Windthrow adds topographic roughness to hillslopes by creating pit-mound couplets that are initially sharp in form and degrade with time due to creep-like processes operating within the soil mantle (Fig. 1*A*) (6, 10, 25). At any time t, a hillslope's roughness reflects the balance between the time series of roughness production by windthrow and persistent decay of that roughness by creep-like processes. Windthrow production is a stochastic signal driven by atmospheric extremes, which are difficult to measure (26). Satellite imagery has been used to map blowdown events in the Amazon Rainforest (27); however, these studies are normally limited to forest disturbances that are hectares in size and one cannot determine whether trees have snapped or been uprooted. Many windthrow events in temperate settings involve a small number of trees and are not easily observable using satellite imagery. Lidar surveys may be used to map tree gap sizes (28) at fine scales, but these also do not distinguish between windthrow and other forms of tree mortality. Further, repeat lidar surveys over large areas are rare, which prevents direct measurement of windthrow events. In this paper, we develop the statistical relationship between topographic roughness, geomorphic creep-like processes, windthrow occurrence, and extreme wind events and use these relationships to identify the probability function of windthrow production rates (Fig. 1) for a moderate relief and temperate setting.

Author affiliations: [a]Department of Earth and Atmospheric Sciences, Indiana University, Bloomington, IN 47405; and [b]O'Neill School of Public and Environmental Affairs, Indiana University, Bloomington, IN 47405

Author contributions: T.H.D., B.J.Y., and D.A.E. designed research; T.H.D. performed research; K.A.N. provided the wind speed data; T.H.D. analyzed data; and T.H.D., B.J.Y., D.A.E., and K.A.N. wrote the paper.

The authors declare no competing interest.

This article is a PNAS Direct Submission.

[1]To whom correspondence may be addressed. Email: doanet@iu.edu.

This article contains supporting information online at http://www.pnas.org/lookup/suppl/doi:10.1073/pnas.2212105120/-/DCSupplemental.

Published January 9, 2023.

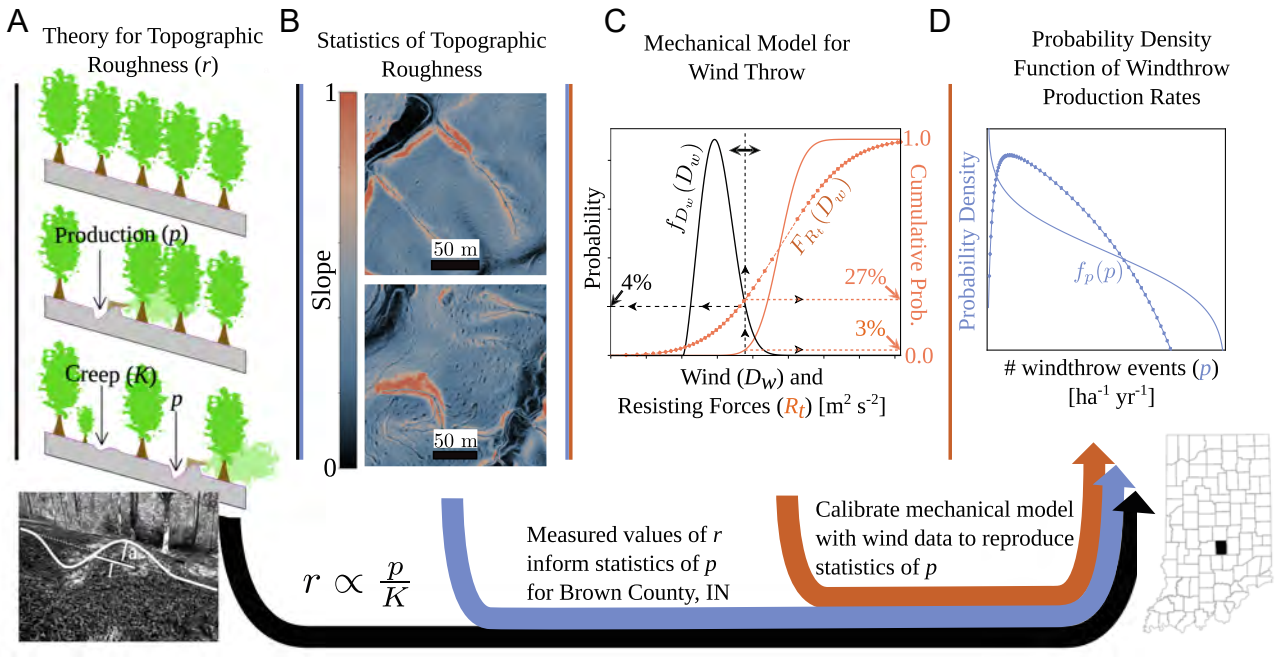

Fig. 1. (*A*) Topographic roughness (r) is directly proportional to the windthrow production rate (p) and inversely proportional to the rate of creep-like decay processes (K). Across sites, this relationship scales with a constant C that describes the pit geometry. The image shows a pit-mound couplet with geometric factors l and a labeled. (*B*) Slope maps (rise over run) from lidar-derived DEMs of two hillslopes with different amounts of roughness due to windthrow, implying different histories between them. (*C*) The mechanical model of windthrow involves calculating the probability of windthrow by determining the overlap between distributions of a driving force (wind gusts, black lines) and resisting force (tree strength, orange lines). The particular overlap of those two distributions produces unique probability functions and statistical moments of windthrow production rates (*D*). Map of Indiana and Brown County are in the lower right of the figure.

We use southern Indiana as a case study and consider a mechanical model, which is capable of recreating surface roughness characteristics similar to what we observe in nature, providing evidence that the theoretical model is rooted in reality. Last, we illustrate the potential for surface roughness to serve as an archive of extreme wind events.

1. Theory

In this section, we present a theory that describes topographic roughness and its statistical relationship to windthrow production rates. Throughout this paper, μ_X and σ_X^2 refer to the mean and variance of the random variable X, respectively. The functions $f_X(X)$ and $F_X(X)$ are the probability density and cumulative probability functions, respectively. The subscript describes the function, which may take different arguments. For example, $F_X(Y)$ describes the probability that a random variable $Y > X$.

A. Topographic Roughness. Windthrow pit-mound couplets add roughness to hillslopes at the scale of meters (Fig. 1 *A* and *B*). Over time, creep-like processes smooth couplets back toward a planar surface (25, 29, 30). The topographic roughness of a hillslope at time t [y] is the sum of topographic variance from all pit-mound couplets of all ages, which amounts to a convolution of the windthrow production rate $p(t)$ [m^{-2} y^{-1}] (number per area per year) with a decay function. Previous work (10) demonstrates that the roughness through time is

$$r(t) = \frac{a^2 w^2 l^2 \pi}{32} \int_{-\infty}^{t} p(t') \left[\frac{l^2}{4} + K[t-t']\right]^{-3/2} \times \left[\frac{w^2}{4} + K[t-t']\right]^{-1/2} \mathrm{d}t', \quad [1]$$

where r [m^2] is the topographic roughness (defined as the variance of elevation), $t - t'$ [y] is the age of couplets, and K [m^2 y^{-1}] is a topographic diffusivity, which is a measure of the magnitude of all creep-like soil transport processes. a [m^2], l [m], and w [m] are product amplitudes and characteristic lengths and widths of initial pit-mound couplet geometry, respectively, defined in ref. 10 (*SI Appendix*). In some settings, burrowing animals (31), shrubs (32), solifluction lobes (33), landslide deposits (34, 35), and bedrock outcrops (36) are sources of topographic roughness. Those roughness sources are not present in our study area, so that windthrow is the primary natural roughening process at the scale of meters (10), as is the case for many moderate relief (10 to 100 m of relief and modest slopes 0.5) and temperate settings (8). We use Eq. **1** to define relationships between statistical moments of topographic roughness and the windthrow production rate.

B. Windthrow Production Rate. On a single hillslope bound by a channel at the base and a ridge at the top, the number of windthrow events per year per hectare, $p(t')$ [m^{-2} y^{-1}], is a noisy time series that we consider as a discrete white noise. Using measured topographic roughness values and theory, we aim to describe and measure the underlying probability distribution, $f_p(p)$ [m^2 y], that the white noise, $p(t')$, samples.

Previous researchers note that newly created forest gaps expose existing trees to greater stress so that their likelihood of failing increases (37, 38). This would add correlation in the time series of p. On the other hand, a very large blowdown event would remove many trees from the hillslope, and another event of the same size is unlikely to occur until the forest recovers, which describes an anticorrelated signal. The consequences of correlation or anticorrelation in p are unclear and are worthy of their own investigation. However, for most of the hillslopes in Brown County, IN, we do not observe evidence for major

windthrow events that create very large canopy gaps, so that white noise is appropriate for our study.

To solve for statistical moments, we rearrange a result from ref. 10 which provides the mean windthrow production rate,

$$\mu_p = \frac{4\left[\phi^2 + \phi\right]}{a^2 l^2 \pi} K \mu_r, \qquad [2]$$

where $\phi = l/w$. We also solve for the relationship between σ_p^2 and σ_r^2 (*SI Appendix*)

$$\sigma_p^2 = \frac{48\phi^4}{a^4 l^2 \pi^2 \Delta t \phi_c} K \sigma_r^2 - \mu_p^2, \qquad [3]$$

where Δt is 1 y and $\phi_c = 1/2\left(\phi^2 + \phi - 1/5\right)$ is a correction factor for when $\phi \neq 1$. A solution exists for $\phi \neq 1$, but it involves many terms, so we provide this approximation for simplicity. The Δt arises because our analytical solution requires that we discretize the problem. Eqs. **2** and **3** show that the mean and variance of windthrow production are linearly related to the mean and variance of topographic roughness respectively and hillslope diffusivity. All components on the right-hand side are measurable from high-resolution topography or are rate constants that can be estimated (e.g., K). Estimating the topographic diffusivity K is challenging, though previous work provides bounds and suggests that K varies with climate (39–42). We consider values of $0.001 \leq K \leq 0.01$ [m^2 y^{-1}].

Land-use history is a complicating factor. As with most of the eastern United States (43), much of Brown County was clear-cut in the 19th century, which may have resulted in smoother topography. However, forests began regenerating on many of these hillslopes in the early 20th century (44, 45), such that the unforested period of these landscapes was relatively brief. While most of Brown County was affected by land-use change, some hillslopes may have been thinned for timber instead of farmed (44). The consequence of land-use history on topographic roughness remains unknown. Previous authors have dated pit-mound couplets to have ages of 100 to 1000 y in heavily logged and mined states of Wisconsin and Michigan (46), and topographic roughness in New England had been attributed to precolonial storms (47). However, agricultural practices that involved intense tilling would have smoothed and reduced natural topographic roughness. We consider two end-member cases. Case A assumes that the roughness persists through land-use change so that there is no memory of land-use change. Case B assumes that the roughness was completely removed during the 19th century and began to accumulate 100 y ago so that there is memory of land-use change. Mathematically, the difference between these two scenarios is captured by the lower limit of integration in Eq. **1** (Case A: $-\infty$ and Case B: $t - 100$ y). We calibrate the mechanical model for Case A using values measured from Eqs. **2** and **3**, for Case B, we use modified forms (*SI Appendix*).

C. Mechanical Model. For a tree to uproot, the drag force must exceed a resisting force (2–5, 7, 48), which involves the strength of roots and soil and the ability of a tree to flex. Resistance strengths vary between individual trees (37, 49) as they differ by rooting depth, degree of sheltering, surface slope, and canopy geometry. The extreme wind events that drive windthrow occur during rare atmospheric events that create highly variable turbulent bursts and sweeps. Therefore, the occurrence of windthrow involves the exceedance of one highly variable quantity (drag force) above another (tree resistance). We approach this as a probabilistic problem where windthrow rates are determined by the overlap of drag and resisting force distributions (Fig.1*C*). Our model does not explicitly resolve the intrastorm dynamics where one windthrow event may lead to others and the formation of canopy gaps. The probabilistic approach is best applied at timescales longer than the storm and is only capable of asking what is the probability that P trees fail given that a maximum wind gust of X meters per second occurred. This allows for the possibility of gap-forming processes. To be clear, probabilistic does not imply random but that our model incorporates the range of wind gusts and the variability of the characteristics that determine trees' resistance to strong winds (e.g., tree species, exposure, height, dbh, etc).

Windthrow occurs during the strongest wind events. We anticipate that derechos, which are large convective wind storms (50), are the primary source of extreme winds in southern Indiana. Tornadoes can affect forests (51, 52) of southern Indiana, but their footprints are smaller and they are comparatively rare. We define the driving force as the square of the strongest three-second gust speed in a year, D_w [m^2 s^{-2}]. Gusts are commonly measured using the 3-s time interval (26), and we use the squared gust speed instead of a drag force because we do not know the values of the coefficients of drag or cross-sectional areas for each tree, which are required to calculate a force (4, 5). In our model, different canopy shapes and sizes (and their impact on drag force) are implicitly incorporated in the resistance function as they impact which wind speeds certain trees can withstand (49). The cumulative distribution function for tree resistance, $F_{R_t}(D_w)$, describes the probability that a tree will have a resistance $R_t < D_w$ [m^2 s^{-2}] and fail. As an example, a forest with a wide variety of canopy shapes, topographic exposure, or rooting depths may have a larger variance in R_t.

The probability distribution of windthrow production rates, p, is determined by the overlap of driving and resisting force distributions. The resistance function $F_{R_t}(D_w)$ describes the portions of trees that cannot resist a certain gust speed and will fail and the rest which will remain standing. For a hillslope with N trees, each tree has the same probability of being from the population of trees that fail. This describes N trials with two outcomes: a windthrow event or not. The binomial distribution captures this description and is the conditional distribution of the number of windthrow events given a gust speed,

$$f_P(P|D_w) = \binom{N}{P} F_{R_t}(D_w)^P \left[1 - F_{R_t}(D_w)\right]^{N-P}, \qquad [4]$$

where $P = pH\Delta t$ is a dimensionless integer that is the number of trees that fall on a hectare, H [m^2], in 1 y, Δt. The remaining piece is to determine how frequently maximum gust speeds have a value between D_w and $D_w + \Delta D_w$, which is given by the probability density function, $f_{D_w}(D_w)\Delta D_w$. Using wind speed data to determine f_{D_w} and the rules of marginal, conditional, and joint probabilities (*SI Appendix*), we are able to obtain the outstanding marginal distribution—the probability distribution of windthrow production rates $f_p(p)$ (Fig. 1*D*).

This approach is flexible and can incorporate physical elements of drag forces, tree roots, topography, and others, and it implicitly incorporates all of the uncertainty and range of these properties. All of these contribute to the variance of R_t, and we can estimate their impact when measured over the spatial scale of 1,000's km^2 (e.g. Brown County, IN). However, Brown County, IN, has relatively uniform rock type, forest characteristics, and physical

geography, which should reduce the variability of tree resistance and wind speeds.

The resistance function, $F_{R_t}(R_t)$ is unknown for any particular landscape and forest, but physical arguments inform some limits on the shape. First, the pdf of tree resistance, $f_{R_t}(R_t)$, must have a finite mode that is greater than the mode of driving forces, which reflects the simple observation that the most common result is that trees resist most winds. Second, we are primarily concerned with the location and spread of tree resistance R_t, which amount to the mean μ_{R_t} [m^2 y^{-2}] and variance $\sigma^2_{R_t}$ [m^4 y^{-4}]. Given these constraints, we postulate that tree resistance is normally distributed so that $F_{R_t}(R_t)$ is an error function. The normal distribution is the maximum entropy distribution for a known mean and variance, meaning that it requires the fewest assumptions about the process, given that we know the first two moments (53). This argument guides our choice as we determine only the first two moments from Eqs. **2** and **3**.

Calibrating the mechanical model with topographic roughness requires that most tree throw in the field area is driven by wind and is therefore windthrow. Tree throw is a more general process and may also be driven by ice loading (54) and root rot (55). In southern Indiana, we observe a clear aspect dependency of tree throw couplets that is consistent with the dominant wind direction (e.g., east and north-facing hillslopes) (10). Furthermore, if ice or root rot were the primary drivers, then we would expect to see approximately uniform occurrence of couplets. But instead, we see variability in topographic roughness (Fig. 2*B*) on different hillslopes and so that tree throw must be driven by something with lots of variance, like wind. Nonetheless, in *SI Appendix*, we develop a purely probabilistic model that does not specify the driving mechanism, which produces results that are similar to the mechanical model.

2. Data

A. Topographic Roughness. Recent work collected r on 1,910 hillslopes from Brown County in southern Indiana (Fig. 1*B*) (10), which is largely forested and hilly with 200 m of relief and locally steep slopes (up to 45°). Flat-lying shales, limestone, and sandstone underly the entire county. We measure topographic roughness from statewide, 0.76-m resolution, topographic data that are fine enough to measure topographic roughness due to windthrow, r (10). For this work, we limit our analysis to hillslopes with slopes between 14° and 33° (0.25 to 0.65 slope) (Fig.1*B*) because shape parameters for pit-mound couplets are consistent throughout moderately steep slopes. On shallow slopes, much of the sediment falls back into the pit, and couplets are small (10, 31). On steeper slopes, the couplets are shallower and longer and contribute differently to topographic variance. This limits our analysis to 1,408 hillslopes. From these data, we obtain $\mu_r = 0.005$ [m^2] and $\sigma_r^2 = 7.14 \times 10^{-06}$ and we calculate μ_p and σ_p^2 using Eqs. **2** and **3** for Cases A and B and for different values of K. These values of μ_p and σ_p^2 inform the mechanical model described above. Data are available in ref. 56.

B. Wind Speed Data. Empirical measurements of extreme wind events are notoriously sparse (18, 57). We used a 20-y record of hourly (2000 to 2020) and 2 y of 10-Hz (2019 to 2020) wind speed measurements from the nearby Morgan-Monroe State Forest AmeriFlux site (US-MMS) to characterize the distribution of wind gusts in the region (58). The tower is located on a ridge at 39.3232 N, 86.4131 W. At 46 m tall, it is 20 m above the canopy which has an average height of 27 m and is composed of 80 to 90-y-old deciduous trees that are sugar maple, tulip poplar, sassafras, and oaks (59). We think that the statistics from this site are representative of Brown County, which has consistent topographic relief so that there are not any orographic or systematic topographic routing issues. Pairing maximum gust values per hour with the hourly average results in 17,520 measurements. Using those data, we form a statistical relationship between gust speeds and hourly averaged speeds and apply the statistical relationship to the full 20-y record of hourly wind speeds (Fig. 2). Data are available in ref. 56.

We first define the form of the probability distribution of hourly averaged wind speeds, u_h [m s^{-1}], which is a mixture of Weibull and Gumbel distributions weighted by ≈3/4 and ≈1/4, respectively, and summed together (Fig. 2*A*). The Weibull (60) and Gumbel distributions have both been used to describe wind speed distributions, with some noting that the Gumbel provides a better fit to the tail (61). Next, using 2 y of 3-s averaged wind speeds (gusts), we define the statistical relationship between the probability of maximum squared gust speed, u_g^2 [m^2 s^{-2}], given an hourly averaged wind speed (Fig. 2*B*, yellow contours). The mean of the conditional distribution of $f_{u_g^2}(u_g^2|u_h)$ is similar to the gust factor referenced in other studies (3). We find that

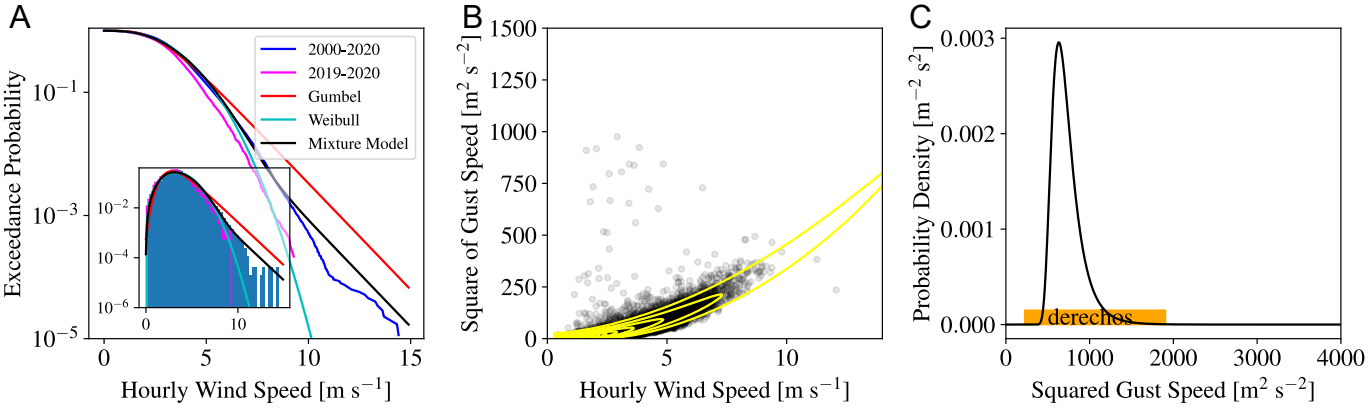

Fig. 2. (*A*) Magenta and blue are data from 2019–2020 and 2000–2020 respectively. Exceedance probability and probability density function (inset) of hourly averaged wind speed data from the Morgan Monroe AmeriFlux tower. We test Gumbel (red), Weibull (cyan), and a mixture model of the two (black). (*B*) The relationship between squared gust speed and hourly averaged wind speed allows us to develop the distribution of gust speeds. Yellow lines are the contours of the joint probability of hourly wind speed and maximum squared gust speed, which we use to construct the extreme value distribution. (*C*) Probability density function of the square of the most extreme wind gust speed in a year. The derived extreme value distribution appears to overlap with reported gust speeds for derechos (50).

the maximum gust, u_g, is, on average, 1.9 times the hourly average (*SI Appendix*). Typical gust factors range between 1.4 and 2.8, so that our estimate of 1.9 is consistent with average gust factors across the conterminous United States (26) and at sites in the United Kingdom (62). Using the rules for marginal, conditional, and joint probabilities, we determine the probability distribution of 3-s averaged squared gust speeds (A1). Finally, we generate the extreme value distribution of 3-s squared gust speeds, f_{D_w} (Fig. 2*C*) (A2). The resulting form for f_{D_w} overlaps with reported values for squared gust speeds from derechos, which are a significant source of extreme winds in southern Indiana (50, 63) (Fig. 2*C*). In the next section, we combine the theory and roughness data to obtain $f_p(p)$.

3. Results

A. Mechanical Model. We calibrate the mechanical model by iteratively adjusting the position and spread of the resistance function, $F_{R_t}(R_t)$, to change the overlap with the driving force distribution, $f_{D_w}(D_w)$. This leads to different forms of $f_p(p)$ (Fig. 1 *C* and *D*). We then select the combination that produces $f_p(p)$ with μ_p and σ_p^2 that best match measurements from Brown County. We test different land-memory cases and use different topographic diffusivities, but in all cases, the results show small, but nonzero, probability of windthrow for typical annual wind speed maximum (20 ms^{-1}) in this region (Fig. 3*A*). The probability of failure increases significantly once severe storm or tornadic wind speeds are surpassed.

Both land-memory case (A & B, dotted lines) and topographic diffusivity, K (colors), affect the distribution, $F_{R_t}(R_t)$ (Fig. 3*A*). Small values of K (yellow) require resistant trees because topographic roughness decays slowly. Therefore, in order to create the roughness statistics that we observe in Indiana, the production rate must be low. There are also differences between land-memory cases. In general, F_{R_t} must be shifted toward weaker resistance values for Case B (land-memory, roughness removal) as compared to Case A (no land-memory, roughness persistence). This results in higher values of μ_p and is most pronounced for $K = 0.001$ (Fig. 3*D*). This is because systems with large topographic diffusivities approach an expected steady-state roughness value faster than those with small diffusivities. In *SI Appendix*, we parameterize a Weibull distribution using the method of moments and Eqs. **2** and **3**. This method does not assume any particular driving mechanism and is a general approach, but results from this analysis are consistent with our mechanical model (Fig. 3*B*, dotted lines). In general, mean values

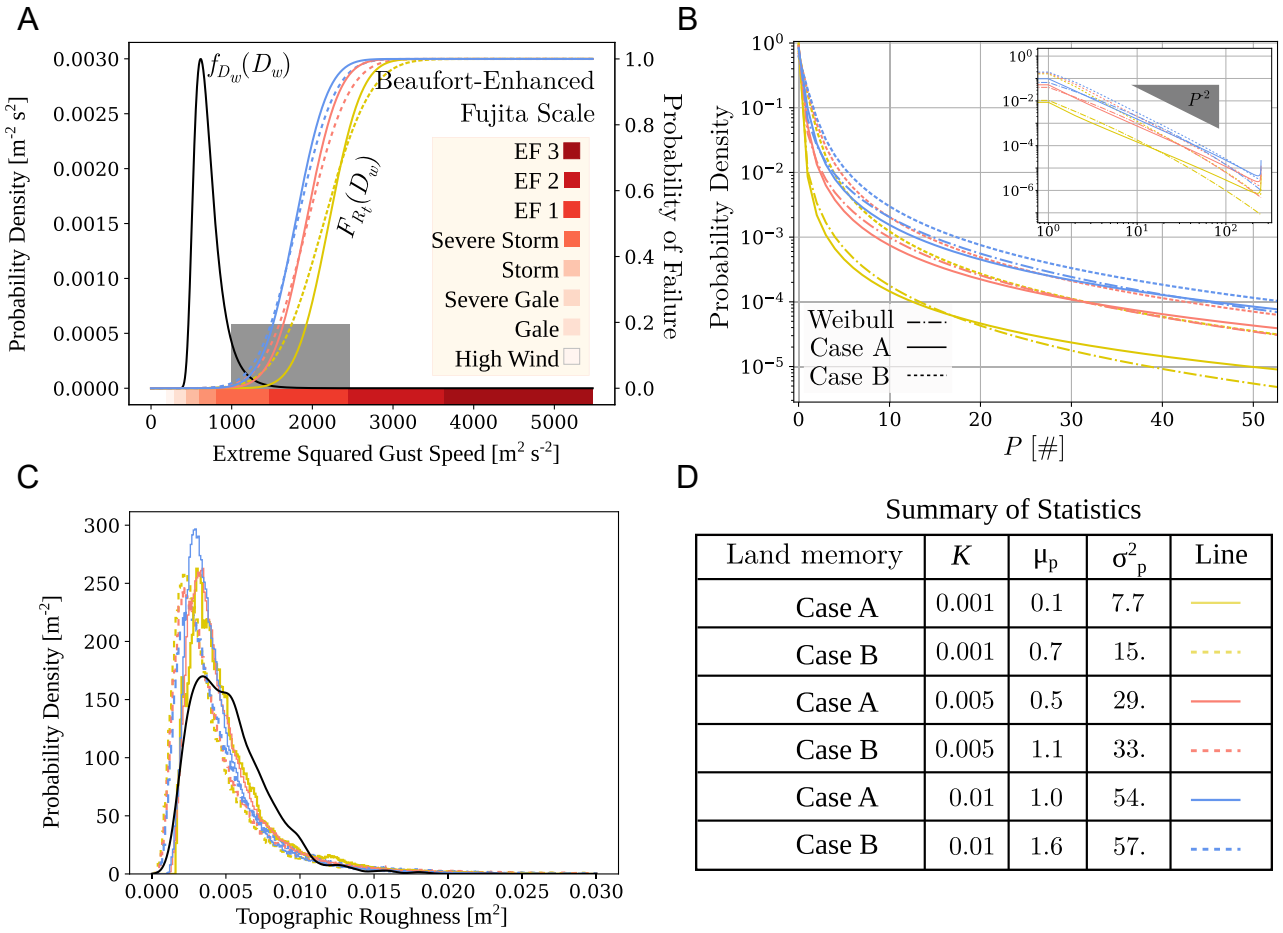

Land memory	K	μ_p	σ_p^2	Line
Case A	0.001	0.1	7.7	
Case B	0.001	0.7	15.	
Case A	0.005	0.5	29.	
Case B	0.005	1.1	33.	
Case A	0.01	1.0	54.	
Case B	0.01	1.6	57.	

Fig. 3. (*A*) Overlap of driving forces (black) and the cumulative distribution of resisting forces (colors) which should be interpreted as the conditional probability of failure given a driving force. We show best-fit forms of resistance functions for three values of K and using a normal distribution for resistance strengths. The gray box illustrates the range of previous estimates of probability of failure given a squared wind speed from refs. 64 and 65. We also note that our resistance function is consistent with that used in the model by Godfrey and Peterson (2017). (*B*) The resulting probability distribution of windthrow production rates calculated by the overlap of driving and resisting forces in (*A*) and using the method of moments for a Weibull distribution. (*C*) Probability distribution of numerically simulated roughness values from Eq. **1**, where p is drawn from $f_p(p)$ in (*B*). The black line is the distribution of measured roughness values weighted by hillslope area. (*D*) Table of results and statistics for the probability distributions in (*B*).

of P range from 0.1 to 1.6, depending on diffusivity and land-memory case, which are consistent with previous studies (7).

To evaluate the feasibility of $f_p(p)$, we numerically simulate Eq. **1**, (*SI Appendix*) and draw $p(t')$ from our best-fit probability distributions. In general, results for runs from Case A appear to perform better than Case B, which may indicate that not all roughness was removed in the 18th and 19th centuries (Fig. 3*C*). But for all cases, the approximate location and spread of the simulated distributions are close to those of the observed distribution.

B. Climate Forcing. One of the many consequences of a warming climate is a likely shift in magnitude or frequency of extreme weather events. For example, tropical cyclone frequency may decline while the intensity may increase (66). There is significant uncertainty, however, regarding how wind speeds will change in different climate change scenarios and locations. There is some evidence that wind speeds are declining in North America (18), while at the same time, there is evidence that winds are increasing in parts of Europe (57). While different regions will respond differently to climate change, there remains significant uncertainty around wind speeds partly because there are few natural archives and limited historical data (57).

Using the best-fit forms of F_{R_t} (Case A, $K = 0.005$ for illustration), we consider a possible response of forests to various scenarios. For the moment, we neglect possible changes of tree resistance and focus on shifts in extreme winds. We test six different scenarios that span from −3% to +3% mean extreme wind speeds (note that this is not the square gust speed), which change f_{D_w} by shifting the entire distribution toward lower or higher values. For reference, the average maximum annual gust speed is 26.5 [m s^{-1}], and a 3% change results in ±0.8 [m s^{-1}]. These values are entirely consistent and even conservative compared to previous modeling efforts which suggest that a 6% increase in the 90th percentile of wind speeds (57, 67). Combining these distributions with F_{R_t}, we can explore possible forest responses to changes of extreme wind statistics (Fig. 4*A*).

There is a nonlinear response to changes in extreme wind statistics (Fig. 4*B*), and a 3% increase of the average maximum gust speed drives a 38% increase in μ_p. The overlap of the tails of two distributions, which are nonlinear functions, drive

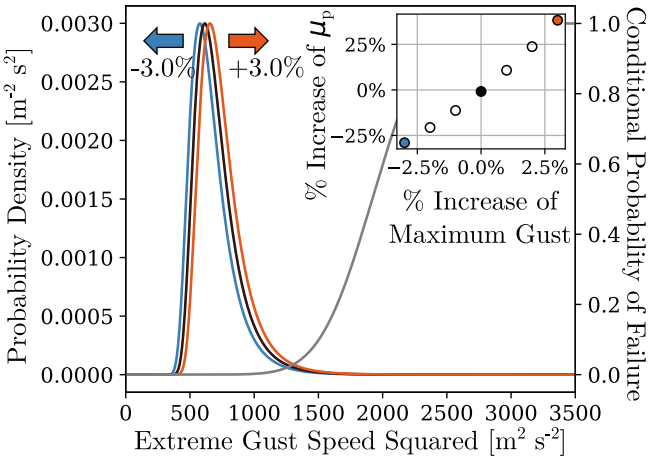

Fig. 4. (*A*) Extreme value distributions of squared gust speed for cases where the extreme gust speed (not squared) ranges from 97% (blue) to 103% (orange) of the baseline values (black) and the resistance function for the case where $K = 0.005$ (gray). (*B*) Resulting mean windthrow production rate for each case.

windthrow and leads to a nonlinear response of μ_p to changes in gust speed. For the case where wind speeds decrease, the windthrow production rate would decline, but at a slower rate than a comparable increase in wind speeds. This analysis neglects possible physical responses of trees.

4. Discussion

A. Coevolution of Wind and Forests. Forests may respond to climatic changes in a number of ways. Trees may increase resistance to mechanical stresses through thigmomorphogenesis (68), or trees may lose resistance following fire (69), or beetle kill and disease may change the entire resistance function by removing certain species (70). The mechanical model can incorporate the coevolution of climate and tree resistance by all of these responses as a shift of $\mu_{R_t}(R_t)$ and $\sigma^2_{R_t}$. For example, an increase of μ_{R_t} which may be accomplished in one of two ways. In the first, an increase of D_w results in a response of all trees to become more resistant, which shifts F_{R_t} toward larger values. In the second, an increase of D_w may rapidly remove the weaker trees, leaving only the resistant ones remaining and thereby shifting F_{R_t} toward larger values as well. In addition to changing the mean and variance of tree resistance, we could also consider the possibility of changing climates adding or changing the skew of tree resistance distributions. We have limited our analysis to distributions with zero skew here because we lack the higher-order information required for higher moments. However, a fruitful avenue for future research may be to combine physics-based models like forestGALES (71) with topographic roughness and our approach here.

B. Topographic Roughness as an Archive. Compared to precipitation and temperature, wind speed lacks a comprehensive natural archive (18). Desert, paleolake, and coastal settings provide natural archives of wind events (72, 73), but no natural archive exists for forested settings. The form of Eq. **1** explicitly writes the roughness as an archive of historical extreme events. Previous researchers have used historical records of tree damage and the enhanced Fujita scale (EF scale) to back out information regarding wind speeds (23, 24). However, the EF-scale is discrete, and this approach does not inform $f_p(p)$ or $F_{R_t}(R_t)$. Insofar as the signature of windthrow remains on the forest floor for centuries (46), roughness has the potential for extending modern wind speed data back several more decades or centuries.

In order to realize topographic roughness as an archive, we must address several issues. First, while the topographic diffusivity is a central parameter of theory in this paper, estimating the topographic diffusivity remains a central challenge in geomorphology. Second, the probability distribution of windthrow resistance strengths must be refined. We see opportunities to employ deterministic physical and numerical, e.g., ForestGALES (37, 71) models of windthrow (2–4) within a probabilistic framework (49). Third, a more precise account of land-use change and the impact on topographic roughness should be established. Despite these issues, we reiterate that Eq. **1** unambiguously writes roughness as an archive of historical wind events, which is otherwise lacking.

C. Roughness as a Measure of Carbon Stocks and Fluxes. Nature-based climate solutions require robust strategies to not only quantify present-day carbon uptake but also to project how future climate feedback might threaten the permanence of ecosystem carbon pools and especially carbon stored in tree

biomass. Forest disturbances like windthrow are stochastic, rare events, which has challenged prior attempts to quantify the consequences of wind-driven tree mortality (20). The approach demonstrates that land-surface roughness serves as a record of historical events and thus may be used to fill in the small sample size. Moreover, we demonstrate that even small changes in wind speed distributions may drive large changes in the expected windthrow production rate, which should motivate future work to consider the risk of wind-driven tree mortality in assessments of carbon stored in forest-based NbCS.

5. Conclusions

We leverage theory that uses topographic roughness and lidar data to establish candidate probability distributions of the tree throw production rate, p. Assuming that most tree throw is driven by wind, we find that the distribution of tree resistances must be greater than the distribution of driving forces, with only the tails of the distributions overlapping. The expected maximum gust in Brown County, IN, is 26.5 m s^{-1}, and the average tree can withstand wind speeds of 46, 43, or 42 m s^{-1} (Fig. 3*A*), which relate to the average number of tree throw events ranging from 0.1 to 1.6 events per year, depending on the topographic diffusivity. These values are consistent with previous modeling efforts (7) and tree census studies (64, 66). Our results and methodology are most relevant to moderate relief and temperate settings, but the theory could be adapted to flatter forested settings. Steep settings tend to be roughened by other processes, and it may be challenging to isolate roughness due to windthrow.

We also consider climate change scenarios wherein the average extreme gust in a year increases/decreases by up to 3.0%. Because windthrow is driven by the overlap of nonlinear tails of two distributions, there is a nonlinear response in the frequency of windthrow. For example, a 3.0% increase of average wind gust speed drives a 38% increase in windthrow production. This analysis does not consider any change in the tree population; however, our model can incorporate potential changes by shifting the resistance function.

Last, the theory demonstrates that roughness is an archive of extreme events and suggests that there is potential for using roughness as an archive of extreme wind speeds, which is otherwise lacking. While much work needs to happen for this to be realized, the theory unambiguously writes roughness as an archive. As increasingly high-resolution topographic, climate, and ecological datasets emerge, we suggest that presenting topographic roughness as an accumulated history of events and processes (as in Eq. **1**) will become an increasingly useful tool for quantifying stochastic ecogeomorphic processes.

A. Rules of Marginal, Conditional, and Joint Probabilities. The rules for marginal, conditional, and joint probability functions are critical for this paper. The equations

$$f_{X,Y}(X, Y) = f_X(X|Y)f_Y(Y) = f_Y(Y|X)f_X(X), \quad [5]$$

and

$$f_X(X) = \int f_{X,Y}(X, Y)\mathrm{d}Y, \quad [6]$$

summarize the key relationships.

B. Extreme Value Distribution. The distribution of 3-s averaged wind speeds is nontrivial. The bulk of the distribution may be fit with a Weibull distribution. The tail, however, appears to depart from a Weibull distribution. We have tested a mixture model for the probability distribution of 3-s-averaged wind speeds and note that a model containing Weibull and Gumbel distributions weighted by 3/4 and 1/4, respectively, fits both the bulk and tail well. Describing the tail of the wind speed distribution correctly is key for determining the extreme value distribution.

$$g_v(v) = NF_v(v)^{N-1}f_v(v). \quad [7]$$

In our case, $N = 8{,}760$, which is the number of hours in a year.

Data, Materials, and Software Availability. Probability distributions of topographic roughness and codes for generating f_p are archived at Zenodo (https://doi.org/10.5281/zenodo.6822595) (56).

ACKNOWLEDGMENTS. T.H.D., B.J.Y., and D.A.E. acknowledge support from the Indiana University Environmental Resilience Institute, the Indiana University Faculty Research Support Program, and NSF EAR-2218293. K.A.N. acknowledges support from the AmeriFlux Management Project, administered by Lawrence Berkeley National Lab.

1. J. J. Finnigan, "The Turbulent Wind in Plant and Forest Canopies" in *Plant Disturbance Ecology* (Elsevier, 2021), pp. 17–63.
2. H. Peltola, S. Kellomäki, H. Väisänen, V. P. Ikonen, A mechanistic model for assessing the risk of wind and snow damage to single trees and stands of Scots pine, Norway spruce, and birch. *Can. J. For. Res.* **29**, 647–661 (1999).
3. A. England, C. Baker, S. Saunderson, A dynamic analysis of windthrow of trees. *Forestry* **73**, 225–238 (2000).
4. C. P. Quine, B. A. Gardiner, Understanding how the interaction of wind and trees results in windthrow, stem breakage, and canopy gap formation. Plant Disturbance Ecology: The Process and the Response, (2007), pp. 103–105.
5. B. Gardiner, P. Berry, B. Moulia, Wind impacts on plant growth, mechanics and damage. *Plant Sci.* **245**, 94–118 (2016).
6. E. J. Gabet, S. M. Mudd, Bedrock erosion by root fracture and tree throw: A coupled biogeomorphic model to explore the humped soil production function and the persistence of hillslope soils. *J. Geophys. Res.: Earth Surf.* **115**, F04005 (2010).
7. J. A. Constantine, M. J. Schelhaas, E. Gabet, S. M. Mudd, Limits of windthrow-driven hillslope sediment flux due to varying storm frequency and intensity. *Geomorphology* **175**, 66–73 (2012).
8. J. D. Phillips, P. Amonil, L. Pawlik, J. Trochta, P. Daněk, Domination of hillslope denudation by tree uprooting in an old-growth forest. *Geomorphology* **276**, 27–36 (2017).
9. P. Šamonil *et al.*, Soil denudation rates in an old-growth mountain temperate forest driven by tree uprooting dynamics, central Europe. *Land Degrad. Dev.* **31**, 222–239 (2020).
10. T. H. Doane, D. Edmonds, B. J. Yanites, Q. Lewis, Topographic roughness on forested hillslopes: A theoretical approach for quantifying hillslope sediment flux from tree throw. *Geophys. Res. Lett.* **48**, e2021GL094987 (2021).
11. G. Hancock, J. Lowry, Quantifying the influence of rainfall, vegetation and animals on soil erosion and hillslope connectivity in the monsoonal tropics of northern Australia. *Earth Surf. Process. Landforms* **46**, 2110–2123 (2021).
12. R. J. Schaetzl, S. F. Burns, D. L. Johnson, T. W. Small, Tree uprooting: Review of impacts on forest ecology. *Vegetatio* **79**, 165–176 (1988).
13. D. M. Marra *et al.*, Large-scale wind disturbances promote tree diversity in a central Amazon forest. *PloS One* **9**, e103711 (2014).
14. N. G. Ulanova, The effects of windthrow on forests at different spatial scales: A review. *For. Ecol. Manag.* **135**, 155–167 (2000).
15. M. Valtera, R. J. Schaetzl, Pit-mound microrelief in forest soils: Review of implications for water retention and hydrologic modelling. *For. Ecol. Manag.* **393**, 40–51 (2017).
16. D. S. Schimel *et al.*, Recent patterns and mechanisms of carbon exchange by terrestrial ecosystems. *Nature* **414**, 169–172 (2001).
17. A. Lindroth *et al.*, Storms can cause Europe-wide reduction in forest carbon sink. *Glob. Chang. Biol.* **15**, 346–355 (2009).
18. S. Pryor *et al.*, Wind speed trends over the contiguous United States. *J. Geophys. Res.: Atmos.* **114** (2009).
19. R. Seidl *et al.*, Forest disturbances under climate change. *Nat. Clim. Change* **7**, 395–402 (2017).
20. W. R. Anderegg *et al.*, Climate-driven risks to the climate mitigation potential of forests. *Science* **368**, eaaz7005 (2020).
21. K. A. Novick *et al.*, Informing nature-based climate solutions for the United States with the best-available science. *Glob. Change Biol.* **28**, 3778–3794 (2022).
22. K. S. Hemes, B. R. Runkle, K. A. Novick, D. D. Baldocchi, C. B. Field, An ecosystem-scale flux measurement strategy to assess natural climate solutions. *Environ. Sci. Technol.* **55**, 3494–3504 (2021).
23. L. A. Schulte, D. J. Mladenoff, Severe wind and fire regimes in northern forests: Historical variability at the regional scale. *Ecology* **86**, 431–445 (2005).
24. L. E. Frelich, E. J. Ostuno, Estimating wind speeds of convective storms from tree damage. *E-J. Severe Storms Meteorol.* **7**, 1–19 (2012).

25. Y. Martin, E. Johnson, O. Chaikina, Interplay between field observations and numerical modeling to understand temporal pulsing of tree root throw processes, Canadian rockies, Canada. *Geomorphology* **200**, 89–105 (2013).
26. F. Letson, S. Pryor, R. Barthelmie, W. Hu, Observed gust wind speeds in the coterminous United States, and their relationship to local and regional drivers. *J. Wind Eng. Ind. Aerod.* **173**, 199–209 (2018).
27. R. I. Negrón-Juárez *et al*., Windthrow variability in central Amazonia. *Atmosphere* **8**, 28 (2017).
28. C. R. Reis *et al*., Forest disturbance and growth processes are reflected in the geographic distribution of large canopy gaps across the Brazilian Amazon. *J. Ecol.* **10**, 2971–2983 (2022).
29. R. Jyotsna, P. K. Haff, Microtopography as an indicator of modern hillslope diffusivity in arid terrain. *Geology* **25**, 695–698 (1997).
30. D. J. Furbish, S. Fagherazzi, Stability of creeping soil and implications for hillslope evolution. *Water Res. Res.* **37**, 2607–2618 (2001).
31. E. J. Gabet, O. J. Reichman, E. W. Seabloom, The effects of bioturbation on soil processes and sediment transport. *Ann. Rev. Earth Planet. Sci.* **31**, 249–273 (2003).
32. S. L. Worman, D. J. Furbish, A probabilistic, biologically informed model of desert shrub population dynamics with the granularity appropriate for geomorphic simulations. *Earth Surf. Process. Landforms* **44**, 1221–1232 (2019).
33. J. Del Vecchio *et al*., Record of coupled hillslope and channel response to Pleistocene erosion and deposition in a sandstone headwater valley, central Pennsylvania. *Bulletin* **130**, 1903–1917 (2018).
34. S. R. LaHusen, A. R. Duvall, A. M. Booth, D. R. Montgomery, Surface roughness dating of long-runout landslides near Oso, Washington (USA), reveals persistent postglacial hillslope instability. *Geology* **44**, 111–114 (2016).
35. A. M. Booth, S. R. LaHusen, A. R. Duvall, D. R. Montgomery, Holocene history of deep-seated landsliding in the North Fork Stillaguamish River valley from surface roughness analysis, radiocarbon dating, and numerical landscape evolution modeling. *J. Geophys. Res.: Earth Surf.* **122**, 456–472 (2017).
36. D. T. Milodowski, S. M. Mudd, E. T. A. Mitchard, Topographic roughness as a signature of the emergence of bedrock in eroding landscapes. *Earth Surf. Dyn.* **3**, 483–499 (2015).
37. Y. Y. Chen *et al*., Simulating damage for wind storms in the land surface model ORCHIDEE-CAN. *Geosci. Model Dev.* **11**, 771–791 (2018).
38. S. Dupont, Y. Brunet, Impact of forest edge shape on tree stability: A large-eddy simulation study. *Forestry* **81**, 299–315 (2008).
39. J. T. Perron, P. W. Richardson, K. L. Ferrier, M. Lapôtre, The root of branching river networks. *Nature* **492**, 100–103 (2012).
40. L. Ma *et al*., Regolith production and transport in the susquehanna shale hills critical zone observatory, part 1: Insights from u-series isotopes. *J. Geophys. Res.: Earth Surf.* **118**, 722–740 (2013).
41. P. W. Richardson, J. T. Perron, N. D. Schurr, Influences of climate and life on hillslope sediment transport. *Geology* **47**, 423–426 (2019).
42. R. D. Madoff, J. Putkonen, Global variations in regional degradation rates since the last glacial maximum mapped through time and space. *Q. Res.* **109**, 128–140 (2022).
43. K. Novick *et al*., The drought response of eastern US oaks in the context of their declining abundance. *BioSci.* **72**, 333–346 (2022).
44. M. A. Jenkins, G. R. Parker, Changes in the forest landscape of the Charles C. Deam wilderness, southern Indiana, 1939–1990. *Nat. Areas J.* **20**, 46–55 (2000).
45. M. A. Jenkins, The history of human disturbance in forest ecosystems of southern Indiana (2013).
46. R. J. Schaetzl, L. R. Follmer, Longevity of treethrow microtopography: Implications for mass wasting. *Geomorphology* **3**, 113–123 (1990).
47. S. H. Spurr, Forest associations in the Harvard Forest. *Ecol. Monogr.* **26**, 245–262 (1956).
48. C. Gromke, Wind tunnel model of the forest and its Reynolds number sensitivity. *J. Wind Eng. Ind. Aerod.* **175**, 53–64 (2018).
49. C. M. Godfrey, C. J. Peterson, Estimating enhanced Fujita scale levels based on forest damage severity. *Weather Forecast.* **32**, 243–252 (2017).
50. R. H. Johns, W. D. Hirt, Derechos: Widespread convectively induced windstorms. *Weather Forecast.* **2**, 32–49 (1987).
51. C. J. Peterson, Catastrophic wind damage to North American forests and the potential impact of climate change. *Sci. Total Environ.* **262**, 287–311 (2000).
52. J. D. Phillips, D. A. Marion, A. V. Turkington, Pedologic and geomorphic impacts of a tornado blowdown event in a mixed pine-hardwood forest. *Catena* **75**, 278–287 (2008).
53. D. J. Furbish, S. G. Williams, D. L. Roth, T. H. Doane, J. J. Roering, Rarefied particle motions on hillslopes-part 2: Analysis. *Earth Surf. Dyn.* **9**, 577–613 (2021).
54. M. C. Hellmer, B. A. Rios, W. B. Ouimet, T. R. Sibley, Ice storms, tree throw, and hillslope sediment transport in northern hardwood forests: Sediment transport by tree throw during icestorms in temperate forests. *Earth Surf. Process. Landforms* **40**, 901–912 (2015).
55. P. Greenwood, J. Bauer, N. J. Kuhn, Assessing hillslope sediment generation potential by tree throw: A preliminary field study along a small river valley in the Jura mountains, northwest Switzerland. *Geog. Helv.* **76**, 319–333 (2021).
56. T. H. Doane, D. Edmonds, B. Yanites, K. Novick, Hillslope roughness reveals forest sensitivity to extreme winds. Zenodo. 10.5281/zenodo.6822595. Deposited 12 July 2022.
57. S. Pryor *et al*., Analyses of possible changes in intense and extreme wind speeds over northern Europe under climate change scenarios. *Clim. Dyn.* **38**, 189–208 (2012).
58. K. Novick, R. Phillips, AmeriFlux BASE US-MMS Morgan Monroe State Forest, Ver. 21-5, AmeriFlux AMP (Dataset), 10.17190/AMF/1246080 (2022).
59. D. Roman *et al*., The role of isohydric and anisohydric species in determining ecosystem-scale response to severe drought. *Oecologia* **179**, 641–654 (2015).
60. P. Wais, A review of Weibull functions in wind sector. *Renew. Sustain. Energy Rev.* **70**, 1099–1107 (2017).
61. A. Sarkar, S. Singh, D. Mitra, Wind climate modeling using Weibull and extreme value distribution. *Int. J. Eng. Sci. Technol.* **3**, 100–106 (2011).
62. J. Ashcroft, The relationship between the gust ratio, terrain roughness, gust duration and the hourly mean wind speed. *J. Wind Eng. Ind. Aerod.* **53**, 331–355 (1994).
63. S. F. Corfidi, M. C. Coniglio, A. E. Cohen, C. M. Mead, A proposed revision to the definition of "derecho". *Bull. Am. Meteorol. Soc.* **97**, 935–949 (2016).
64. J. Y. Pontailler, A. Faille, G. Lemée, Storms drive successional dynamics in natural forests: A case study in Fontainebleau forest (France). *Forest Ecol. Manag.* **98**, 1–15 (1997).
65. T. Usbeck *et al*., Wind speed measurements and forest damage in Canton Zurich (Central Europe) from 1891 to winter 2007. *Int. J. Clim.: A J. R. Meteorol. Soc.* **30**, 347–358 (2010).
66. K. J. Walsh *et al*., Tropical cyclones and climate change. *Wiley Interdiscip. Rev.: Clim. Change* **7**, 65–89 (2016).
67. S. Pryor, R. Barthelmie, E. Kjellström, Potential climate change impact on wind energy resources in northern Europe: Analyses using a regional climate model. *Clim. Dyn.* **25**, 815–835 (2005).
68. V. Bonnesoeur, T. Constant, B. Moulia, M. Fournier, Forest trees filter chronic wind-signals to acclimate to high winds. *New Phytol.* **210**, 850–860 (2016).
69. J. M. Gallaway, Y. E. Martin, E. A. Johnson, Sediment transport due to tree root throw: Integrating tree population dynamics, wildfire and geomorphic response. *Earth Surf. Process. Landforms* **34**, 1255–1269 (2009).
70. P. Šamonil *et al*., Tree mortality may drive landscape formation: Comparative study from ten temperate forests. *Ecosystems*, 1–20 (2022).
71. S. E. Hale *et al*., Comparison and validation of three versions of a forest wind risk model. *Environ. Modell. Softw.* **68**, 27–41 (2015).
72. J. R. Knott *et al*., Paleowind velocity and paleocurrents of pluvial Lake Manly, Death Valley, USA. *Q. Res.* **78**, 363–372 (2012).
73. S. Lindhorst, C. Betzler, The climate-archive dune: Sedimentary record of annual wind intensity. *Geology* **44**, 711–714 (2016).